**Measurement of Soil Stiffness during and
Post Liquefaction**

by

Jingwen Zhao (N)

Fourth-year undergraduate project

in Group D, 2011/2012

I hereby declare that, except where specifically indicated, the work submitted herein is my own original work.

Signature: __________________________ Date: _________________

Technical Abstract

Earthquakes can be tremendously destructive. Being one of the most devastating natural disasters, they usually damage buildings and causes economic lost. The occurrence of an earthquake is a result of sudden release of energy under the earth's crust due to the collision of tectonic plates. It creates vibration and leads to shaking and ground rupture, differential settlement of buildings, cracks on the roads, etc. Soil liquefaction is one of the main contributors to seismic risks. However, the behavior of soil under liquefaction is not fully understood. Therefore, it is important to investigate how the soil behaves during liquefaction under seismic wave and minimize the damages caused.

The purpose of this project is to determine the degradation of soil stiffness due to soil liquefaction. As discussed in Brennan et al (2005), measuring shear wave velocity is an appropriate way to determine the small strain shear modulus by back calculation. For evaluation of large strain shear modulus, the 1 dimensional shear beam model can be applied. Shear modulus can be found by working out the slope of shear strain loop. Shear modulus decreases with the increase in shear strain. Centrifuge tests done by Elgamal et al. (2005) and Brennan et al. (2005) show that the degradation of shear modulus agrees with Hardin and Drnevich (1972).

Data needs to be handled properly, especially for the filtering of the data. Sliding off instruments affect the acceleration recorded. Specific band filter is designed using MATLAB, which gives a neater signal with useful information still preserved.

Experiments were performed on homogenous sand sample and layered sand samples. Excess pore pressure and partial liquefaction in loose sand is clearly recorded and observed. On the other hand, in layered model, there is no obvious excess water pressure during both clay and sand models. This can be a result of insensitive instruments or not strong enough shaking is applied to the model. The settlement of the final soil profile is caused due to the dissipation of excess pore pressure. The visual observation shows a reasonable agreement with parabolic isochrones approximation and Tokimatsu et al.(1987). As water is used as pore liquid, the settlement occurred almost immediately after the shaking. A more viscous fluid can be used for future work.

Shear wave velocity is calculated using simple equation of distance of shear wave over travelling time. Both cross-correlation and direct arrival method were used. In layered models, it if found out that the clay will reduce the amplitude shear wave transmitted and has a significant delay in the shear wave arriving time. The experimental data shows in sand, the shear wave velocity drops significantly in shaking but recovered afterwards and so does the shear modulus. While in clay, the shear wave velocity almost does not change but the shear modulus does degrade. The resulting permanent lose of shear modulus is caused by not taking into account the compaction of sands after shakings. Hardin and Drevench (1972)'s equation tends to overestimate the shear modulus over small shear strain in terms of the results from this project.

By considering the layered sand as one uniform sample, it is found out that the shear wave velocities hence shear modulus before and after shaking behaves more like clay and there is great decrease stiffness. The clay seems to change to soil behaviour although in only takes up one third of the volume. This may be caused as the clay used is far too soft than sand. Stiffer clay may be used to investigate the degree of influence caused by soft soil.

Acknowledgements

I would like to thank Dr G. Madabhushi for his continuous advice and help throughout the project. I would also like to thank Mr. M. Stringer for his guidance on using 1-g shaking table in Schofield Center. Mr. B. Lau and Mr. C. Heron explained me how to use the instruments and calibration method. Mr. R. Adams, Mr. J. Chandler and Mr. C. McGinnie and Mr. K. Penther and other technicians in Schofield Center all kindly offer their help throughout my experiments, which I am very grateful.

Table of Contents

Table of Figures

1 INTRODUACTION

Earthquakes can be tremendously destructive. Being one of the most devastating natural disasters, they usually damage buildings and causes economic lost. The occurrence of an earthquake is a result of sudden release of energy under the earth's crust due to the collision of tectonic plates. It creates vibration and leads to shaking and ground rupture, differential settlement of buildings, cracks on the roads, etc.

1.1 Liquefaction

Liquefaction is a physical process generally under shaking, which causes loss of shear strength and stiffness in saturated soil. Furthermore, it may lead to failure of ground, where the building foundations are and the damages of buildings are unavoidable. Soil liquefaction is one of the main contributors to seismic risks. For example, the 2011 Tōhoku earthquake in Japan causes thousands of deaths and damaging properties, as shown in Figure 1 and 2.

Figure 1 Tilted building after earthquake

Figure 2 Cars trapped in ground due t o soil liquefaction

The earthquake induces compressive waves in longitudinal direction and shear waves in transverse direction. The secondary shear waves, S_h, are transmitted through the soil leading to the movement of soil and distortion of soil structure. Hence, soil liquefaction is induced. Liquefaction generally happens in loose sandy soils, as loose sands tend to compact under shearing while dense soils tend to dilate. In dry and loose soil, when shearing occurs, soil will densify, which results in reduction of its volume. Under saturated conditions, loose soils tend to do the same and drain the water through the voids. However, if the shear loading changes rapidly, i.e. under cyclic loading, and there is no enough time for the volume change and pore pressure dissipation to take place, the soil will be liquefied and behave like viscous fluid rather than soils.

In technical terms, Equation 1 expresses the relationship between total stress, σ, effective stress,σ', and pore pressure, u.

$$\sigma = \sigma' + u \quad \text{Equation 1}$$

As σ is constant, increase in pore pressure due to liquefaction will reduce the effective stress, which is the stress that is effective in bearing the loads. The soil is more vulnerable to failure when effective stress is reduced. Full liquefaction is the event when effective stress, σ', becomes 0, in which the soil lost its bearing capacity completely.

Taking the effects of soil liquefaction into account during the building design stage becomes an increasingly essential requirement. However, the behavior of soil under liquefaction is not fully understood. Therefore, it is important to investigate how the soil behaves during liquefaction under seismic wave and minimize the damages caused.

1.2 Problem definition

The purpose of this project is to determine the degradation of soil stiffness due to soil liquefaction. As discussed in Brennan et al (2005), measuring shear wave velocity is an appropriate way to determine the small strain shear modulus by back calculation. For evaluation of large strain shear modulus, the 1 dimensional shear beam model can be applied (Zeghal and Elgamal(1994)) to achieve this purpose.

Hence, the aims of this project are

- To create saturated soil samples and test them under earthquake loading. Samples were prepared and liquefied by earthquake loading, which is simulated using 1-g shaking table in Schofield Centre.
- To use miniature accelerometers, pore pressure transducers to measure accelerations and pore pressure during liquefaction
- To use the air hammer device to generate S_h wave and measure shear wave velocity both before and during the earthquake loading
- To determine shear modulus degradation before and after liquefaction by back calculation.

2 REVIEW OF LITERATURE

2.1 Cyclic behaviour of loose and dense sand

Ishihara (1985) examined the different behaviours of loose and dense sand in undrained cyclic torsion tests and produced Figure 3.

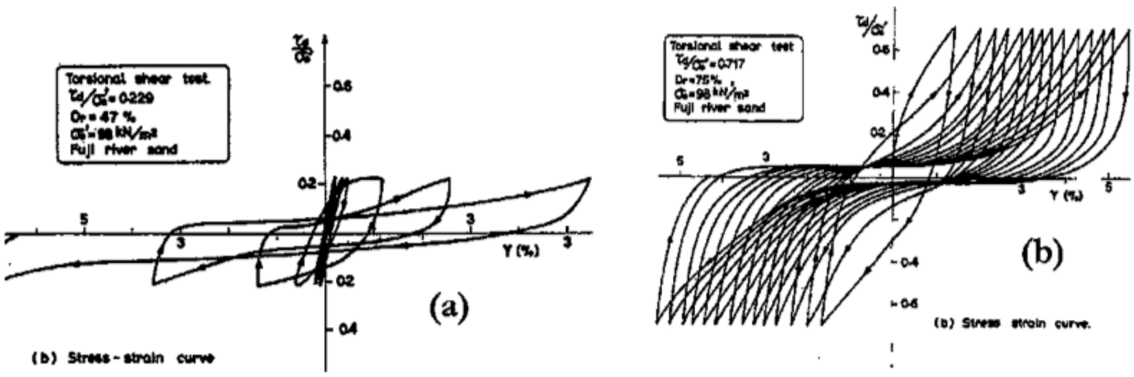

Figure 3 (a) Behaviour of Toyoura sand in undrained cyclic torsion tests (Ishihara 1985) for loose samples (b) Behaviour of Toyoura sand in undrained cyclic torsion tests (Ishihara 1985) for dense samples

Excess pore pressure is built up in both cases. In loose sands, the strain is small initially but is dramatically increased when significant excess pore pressure is generated, which may lead to liquefaction. In dense sand, the sample tends to dilate and the rate at which the shear strain increases is smaller.

For both cases, the shear modulus decreases with the increase in shear strain. Centrifuge tests done by Elgamal et al. (2005) and Brennan et al. (2005) show that the degradation of shear modulus agrees with Hardin and Drnevich (1972), as described by Equation 2, 3, 4 and Figure 4.

$$G = \frac{G_{\max}}{1 + \gamma_h} \qquad \text{Equation 2}$$

where

$$\gamma_h = \frac{\gamma}{\gamma_r}\left[1 + a e^{-b\left(\frac{\gamma}{\gamma_h}\right)}\right] \qquad \text{Equation 3}$$

where $a = -0.2 \ln N, b = 0.16$, N=number of cycles $\gamma_r = \frac{\tau_{\max}}{G_{\max}}$ = reference strain and $$\tau_{\max} = \left[\left(\frac{1+K_0}{2}\sigma'_v \sin\phi'\right)^2 - \left(\frac{1-K_0}{2}\sigma'_v\right)^2\right]^{0.5}$$ Equation 4

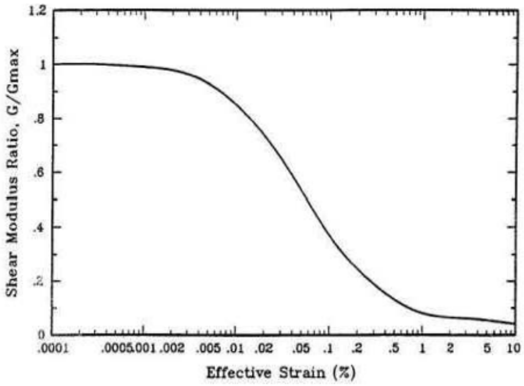

Figure 5 Typical shear modulus degradatino curve by Hardin and Drnevich(1972b)

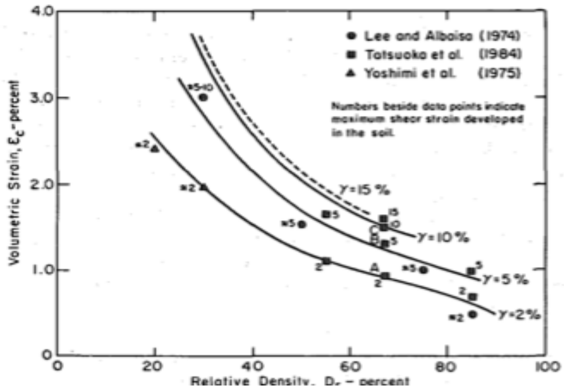

Figure 4 Relationship between volumetric strain, induced strain and relative density for sands (Tokimatsu et al. 1987)

2.2 Settlements due to Earthquake Shaking

When subject to earthquake shakings, soils tend to settle and this is caused by the dissipation of excess pore pressure. Tokimatsu et al. (1987) reviewed previous studies on earthquake-induced settlements of sand and proposed simplified methods to predict these settlements. From laboratory cyclic loading test data, Lee and Albaisa (1974) found that if the sands are not liquefied, the volumetric strain increases as the increase in particle size and excess pore pressure but decreases with increase in relative density. Tatsuoka, et al. (1984) concluded that after initial liquefaction, the effects of soil density and maximum shear strain experienced by the soils are significant. Figure 5 summarize the relationship between volumetric strain, relative density and induced strain in the sands.

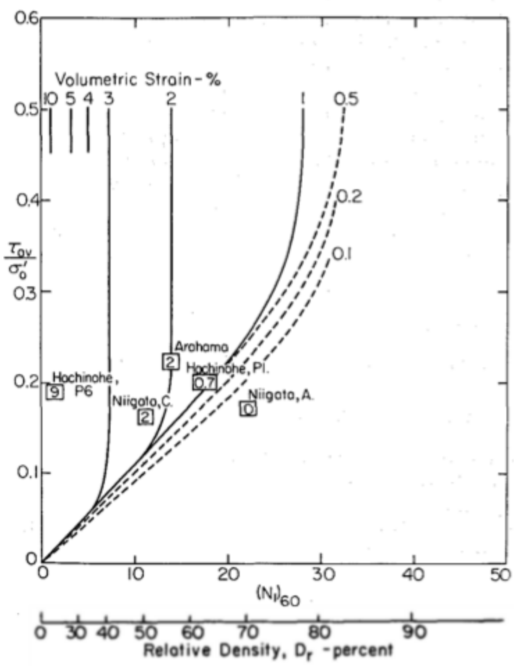

Figure 6 Tentative relationship between cyclic stress ratios, SPT N-values, maximum shear strain and relative density (Tokimatsu et al. 1987)

Based on Seed et al. (1984a), Tokimatsu et al. (1987) gave tentative relationship between cyclic stress ratios, SPT N-value and Maximum shear strain. By combining it with Figure 5 and Meyerhof (1957)'s relationship between relative density and SPT N-value, a chart is proposed for estimating the volumetric strain during cyclic shaking (as shown in Figure 6). Some field data were compared, the existing evidences agree well with the proposed chart although the number of filed data available is limited.

2.3 Evaluation of Shear Modulus

2.3.1 Small strain shear modulus

The estimation of small strain shear modulus can be achieved both numerically and experimentally. The numerical method is based on Hardin and Drnevich equation, as shown in Equation 5

$$G_{\max} = 100 \times \frac{(3-e)^2}{1+e} \times \sqrt{p'} \qquad \text{Equation 5}$$

where e = voids ratio and p' = effective mean confining stress in MPa.

Experimentally, the small strain shear modulus can be calculated by using shear wave velocity according to Equation 6,

$$G_{\max} = V_s^{\,2}\rho \qquad \text{Equation 6}$$

where V_s = shear wave velocity and ρ = bulk soil density.

The number of previous works on evaluating shear wave velocity is limited. Gohl and Finn (1987) and Kita et al. (1996) have used bender elements to detect shear waves in centrifuge models. Ghosh and Madabhushi (2002) have designed an air hammer device to measure shear wave velocity hence evaluate the shear modulus. The air hammer was placed near the bottom and accelerometers were placed in a vertical array. Shear wave will be fired by the air hammer and propagate upwards. Shear wave velocities are calculated from the difference in the shear wave arrival times at adjacent accelerometers, which can be done by direct arrival or cross correlation method. Similar method was used in this project. According to Viggiani and Atkinson (1995), determination of the arrival time of shear wave and shear modulus can be inaccurate due to near field effects if the shear wave only travels through a short distance. This method gives shear strain around 0.03% and it is proved that it will give promising result of G_{max} as the strains are very small.

2.3.2 Shear modulus during earthquake shaking

The shear stress strain behaviour of soil is nonlinear and hysteretic. During the earthquake shaking, shear strain will be too large to apply small strain shear modulus equations. The shear modulus can be obtained by using shear beam equations according to Brennan et al. (2005). The original shear beam equation proposed by Zeghal and Elgamal (1994), Equation 7, relies on the accuracy of surface acceleration measurement.

$$\tau(z) = \int_0^z \rho \ddot{u} dz \qquad \text{Equation 7}$$

However, this data is difficult to achieved as accelerometer is buried in soils at some distance from the surface. Thus, Equation 8 is used to interpolate surface accelerations.

$$\ddot{u}(z) = \ddot{u}_1 + \frac{(\ddot{u}_2 - \ddot{u}_1)}{(z_2 - z_1)}(z - z_1) \qquad \text{Equation 8}$$

Therefore, by combining these two equations, the shear stress can be obtained from Equation 9.

$$\tau(z) = \frac{1}{2}\rho z\left(\ddot{u}(0) + \ddot{u}(z)\right) \qquad \text{Equation 9}$$

Shear strain calculation needs the data of displacements, which can be obtained by integrating the measured value of accelerations. Brennan et al. (2005) suggested starting data recording 0.15s before and a certain amount of the time after the shaking. Forcing these data to be zero when there is no shaking can reduce the noise and unwanted errors. The shear strain can be calculated by first or second expression depending on the number of instruments presented in a given soil layers. If only two instruments are available, first order expression, Equation 10 is suitable. If there are three instruments, a second order expression, Equation 11 can be used, which gives a better estimation.

$$\gamma = \frac{u_2 - u_1}{z_2 - z_1} \qquad \text{Equation 10}$$

$$\gamma(z_i) = \left[(u_{i+1} - u_i)\frac{(z_i - z_{i-1})}{(z_{i+1} - z_i)} + (u_i - u_{i-1})\frac{(z_{i+1} - z_i)}{(z_i - z_{i-1})} \right] \Big/ (z_{i+1} - z_{i-1}) \quad \text{Equation 11}$$

Shear stress-strain loop can be plotted after stress and strain are obtained and shear modulus can be evaluated by examining the gradient of the plot. The most reliable method of finding representative modulus is to evaluate the difference between maximum and minimum stress applied and the difference between maximum and minimum strain developed in the loop, as shown in the dashed line in Figure 7.

By using the method described above, Brennan et al. (2005) found that the shear modulus obtained was appropriate for different soils with some degree of scatter in dry sand. The value of G_{max} calculated from Hardin and Drnevich (1972b) expression was too stiff comparing to the experimental data.

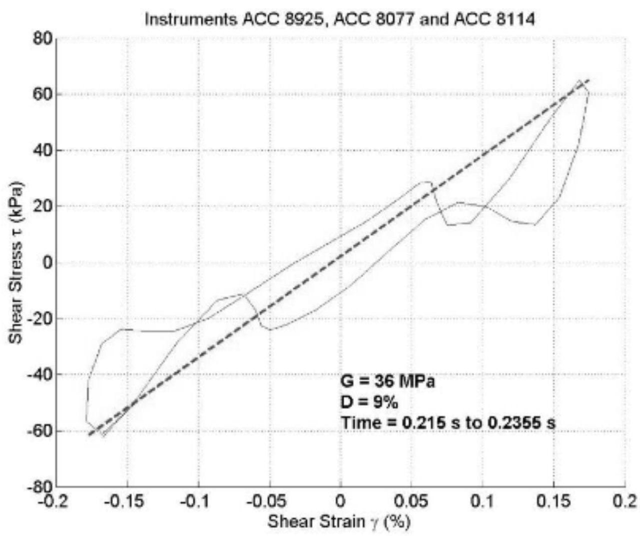

Figure 7 Stress-strain loop for a particular multi-frequency loading of dry sand Brennan et al. (2005)

3 EXPERIMENTAL SET-UP

This section will describe the experimental apparatus and instruments used as well as test procedures undertaken in the experiment stage. All the apparatus and instruments are sensitive. The miniature air hammer described in 3.3.2 is vulnerable to leaking if the air pressure is setting too high. Initial check on air hammer leakage and calibration of instruments prior to the experiments are necessary.

3.1 Shear wave generator

3.1.1 Shaking table

The experiments were operated on a 1-g shaking table in Schofield Center. The motor drives a rotational shaft with an offset mass to generate cyclic loading input. Acceleration of the shaking table can be controlled by varying the offset of the mass. The peak shaking table acceleration is controlled above 0.1g to liquefy the soil simulating the earthquake loading with large shear strain. The shaking table was fired to generate sinusoidal waves at 2, 3, 4hz to the soil model. The shaking table can only generate sinusoidal waves at constant amplitude, frequency and in one horizontal direction at one time. This cannot simulate an exact earthquake signals as real-time earthquakes vary in frequencies, amplitudes and directions.

3.1.2 Miniature air hammer

The miniature air hammer was used to generate small strain shear wave. The air hammer used (as shown in Figure 8) in the experiments is similar to that described in Gosh and Madabhushi (2002) and Randell (2010). It consisted of a hollow brass cylinder capped and fitted with air ports at both ends. A piston is placed inside the brass tube and can only move in longitudinal direction. The air ports are connected to a three way valve, which acts as a switch. The valve is connected to a relay box. It controls the opening side and switching speed of the valves. Air pressure applied through the air ports to the air hammer pushes the piston to quickly stoke towards one end of the cylindrical casing. Every stroke the piston made causes shear wave generated to surrounding soil. Sand was glued to the side of air hammer to increase the coupling between the hammer and surrounding soils.

Figure 8 Miniature air hammer

3.2 Instruments

3.2.1 Accelerometers

According to Randell (2010), MEM accelerometers have good response at low frequencies while piezo accelerometers are more suitable for high frequencies. As the shaking generated will be above or equal to 2hz, piezo accelerometers were used in the experiments.

3.2.2 Pore pressure transducers (PPTs)

1bar PPTs are used to measure the pore pressure generated in the soils. From the data recorded, it gives information on the excess pore pressure generated and the time taken for it to dissipate. The pore pressure measured should not to exceed the range of 1bar to prevent damages of the instruments, especially during calibration process.

3.3 Preparation of soil model

The models were constructed in a rigid steel container with dimensions measured 400mm long, 200mm wide and 500mm tall. There is a glass plate at the front so that the soil deformation can be seen clearly. Models were constructed by pouring dry Huston sand from an overhead manual sand hopper, as shown in Figure 9. The discharge rate and height were carefully controlled to maintain the uniformity of the soil model in terms of relative density, I_D. The discharge rate should be kept high for loose sand. The relative density of the soil was controlled at 40 -50% to provide a liquefiable model. Properties of Hostun sand used are shown in Table 1. Properties of both models, which are discussed later in this report, are shown in Table 2.

Property	e_{min}	e_{max}	Specific gracvity, G_s	Peak friction angle, ϕ'
Value	0.555	1.01	2.65	35°

Table 1 Properties of Hostun sand (from Brennan et al. 2005)

	e	I_D	γ', (kN/m^2)	γ, (kN/m^2)
Hostun sand (homogeneous sample)	0.74	41%	9.3	19.0
Hostun sand (layered sample)	0.655	22%	9.8	19.6
Clay (layered sample)	-	-	9.9	19.9

Table 2 Properties of models

3.3.1 Preparation of homogenous sand samples

Firstly, a depth of 20mm sand was poured before the air hammer was placed at the center. Secondly, the instruments were embedded when the pouring was continued to specific heights and this procedure was then repeated. Accelerometers were placed in a vertical array with a distance of 100mm in between along the central line above the air hammer to pick up maximum shear wave signals. The overall layout of instruments is shown in Figure 10. Finally, the model was saturated by infiltrating water from the bottom through a filter pipe located at the base of the box. This procedure needs to be operated slowly to avoid piping of the model and non-uniform saturation.

Figure 9 Side view of the layout of instruments

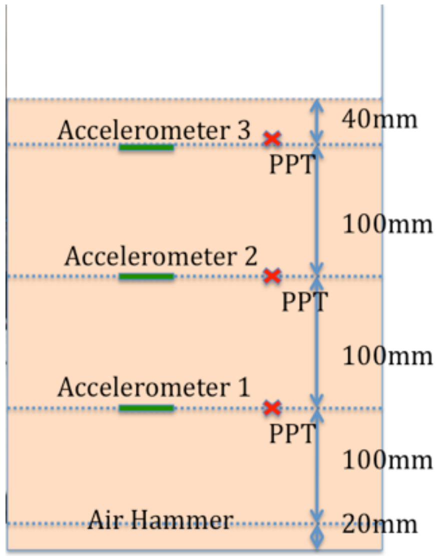

Figure 10 Overhead manual sand hopper

3.3.2 Preparation of layered soil samples

Clay and Hostun sand are used for creating the layered soil sample. Same as homogenous sample, dry Hostun sand was pour to 220mm with instrument embedded. Accelerometer 2 was embedded in sand near the boundary of clay and sand so that the propagation of shear wave in both sand and clay can be evaluate. Clay was then added to top of the dry sand occupying the top 140mm. Finally, the sample was then slowly saturation up to the surface. The reason for saturating the soil last is to prevent the sand to generate excessive pore pressure due to the weight of clay before the shakes.

3.4 Test procedures

Table 3 summarizes test procedures during the experiment. The excitations were carried out in a step-by step manner. It should be noted that the model is no longer at virgin state in Test 3 and 4 as the sample is densified due to previous shaking and the relative density may change slightly.

Phase	**Duration**	**Frequency**	**Comments**
Pre-test			• Calibrate the accelerometers and 1bar PPTs • Prepare soils to specified composition and relative density • Install instruments at required depths • Saturate the soils slowly with water
Test 1	1min		Fire air hammer for evaluation of G_{max}
Test 2	20s	2Hz	• Continue firing air hammer • Fire the shaking table at 2Hz • Stop air hammer at a set of time after the shaking stops
Between shakes	5min		Wait the pore pressure to dissipate
Test 3	20s	3Hz	Repeat Test II but at 3Hz
Between shakes	5min		Wait the pore pressure to dissipate
Test 4	20s	4Hz	Repeat Test II but at 4Hz
Post-test			• Excavate the box and dispose the soil • Recover the instruments carefully • Re-calibrate accelerometers and PPTs

Table 3 Test procedures

4 DATA ACQUISITION AND HANDLING

Accelerometers and PPTs were connected to the data acquisition systems, DASYLab. A sampling rate of 4000hz was used as Ghosh (2004) suggested that the sampling rate should be more than twice the highest frequency of the generated waves. The sliding effect occurs during some of the shaking tests. A filter designed with appropriate frequency chosen significantly reduces the disturbance from this effect and other noises.

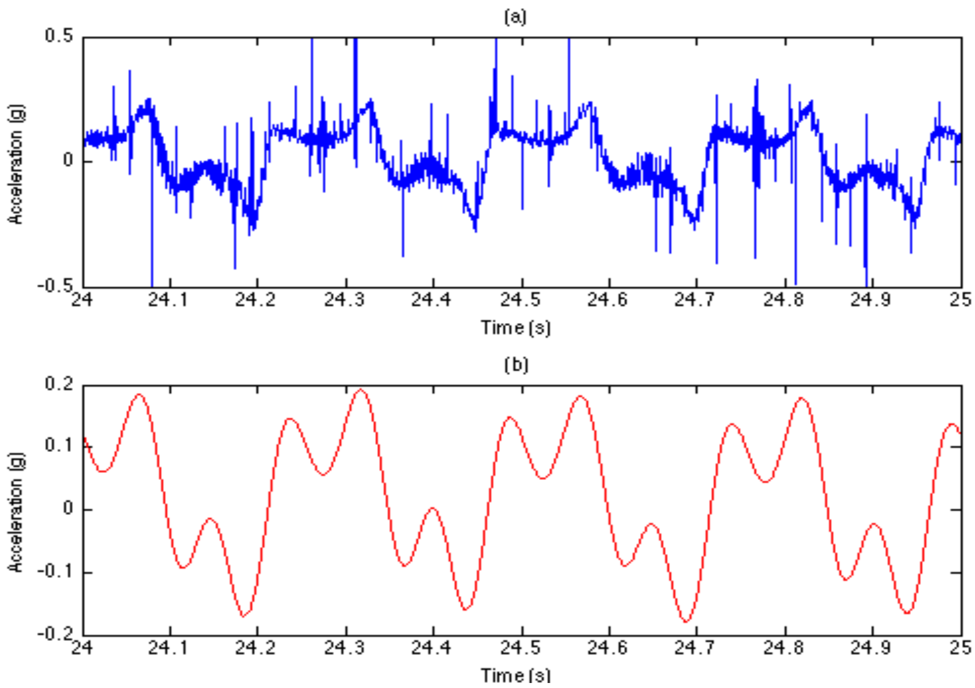

Figure 11 (a) Unfiltered acceleration data at position 1 in 4Hz shaking (b) Filtered acceleration data at position 1 in 4Hz shaking

Figure 11 shows the filtering effects on a typical raw acceleration data recorded in 4hz shaking. During the data acquisition, peizo-acclerometers were used to record accelerations. However, they are sensitive to high frequency signals (Randell (2010)) and tend to pick up high frequency noises. Meanwhile, in strong shakings, instruments embedded in soils did not only tend to settled vertically within the sample, but also slide horizontally with respect to their original positions. This sliding effect will lead to a deformed square waves being recoreded rather than a proper sine waves. As a result, the recorded acceleration in Figure 11(a) appears to be noisy and the shape of sinusoidal cyclic loading response is difficult to recognize. The problem is overcome by employing proper filter. A digital filter is designed using MATLAB (copyright The MathWorks Inc.) code, `[B, A]=butter`

(6,0.0025). Given a sampling rate of 4000hz, the filter will filter out signals over 5hz leaving a main response at 4Hz which is the input shaking table frequency, as shown in Figure 12. Figure 11(b) shows a neater and more sinusoidal-like signal after the filter was applied.

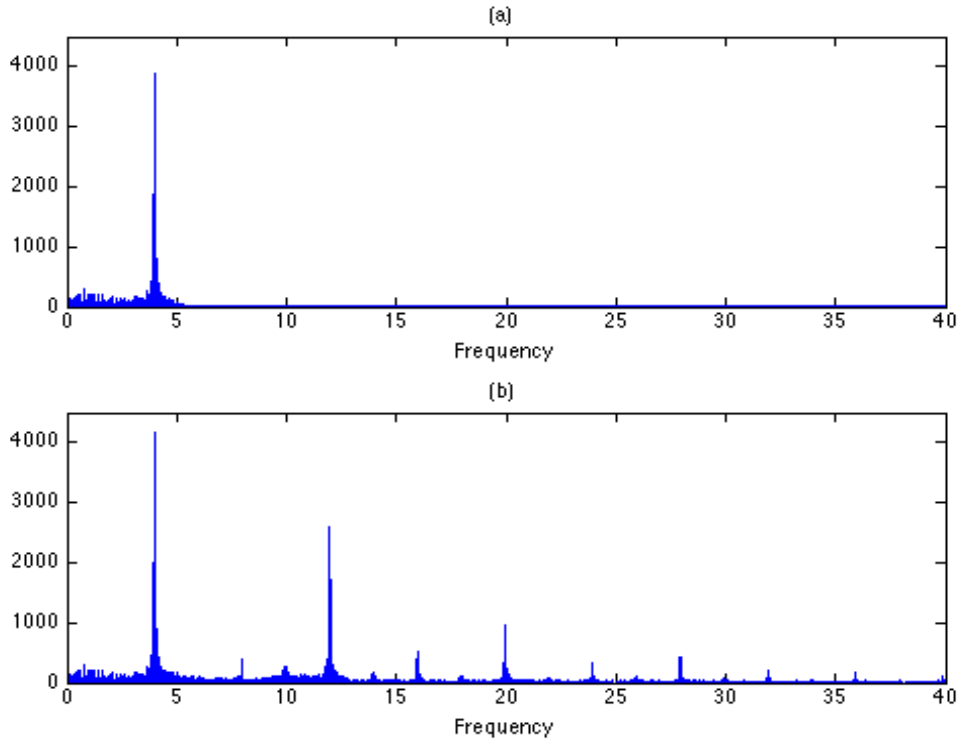

Figure 12 Fourier transform response at position 1 in 4hz shaking for (a) unfiltered acceleration data (b) filtered acceleration data

5 RESULTS OF HOMOGENOUS SAND MODEL

5.1 Excess pore pressure

Pore water pressure accumulation is the reason for liquefaction and the dissipation of the pressure causes settlement. Good evidences were shown that the pore pressure was raised due the shearing. As water is used as pore liquid, the dissipation normally finished very soon after the shaking.

5.1.1 Recorded pore water pressure

Figure 13, 14 and 15 depict the pore water pressure generated in model for 2hz, 3hz and 4hz shaking events respectively. In 2hz and 3hz shakings, very similar pattern is observed. The pore water pressure accumulated up to about 1.56kPa with the maximum value at the deepest position. For positions, refer to Figure 10 in Section 3.3.1. The pore pressure dissipates during the shaking and the time taken is normally in the range of 5 seconds.

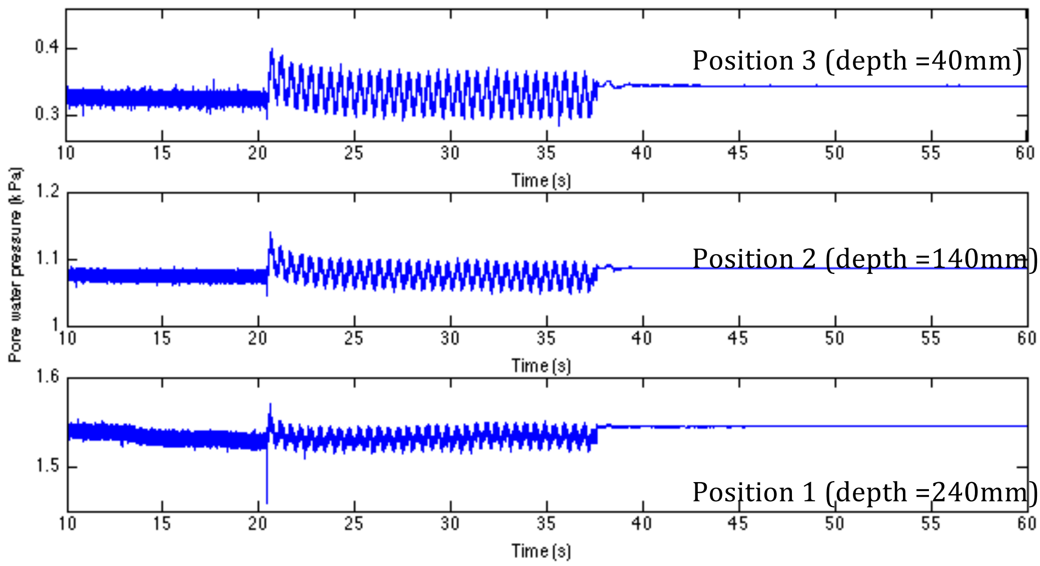

Figure 13 Pore water pressure in 2Hz shaking

During the strongest shaking with 4hz frequency, the accumulation and dissipation in pore pressure is more obvious. There is a significant increase in pore pressure with an unsurprising maximum value of 1.63kPa again at the deepest position. The dissipation time is slightly longer. This phenomenon occurs because that the soil has been compacted due to previous shaking leaving smaller voids. Thus, more time is needed for water to escape.

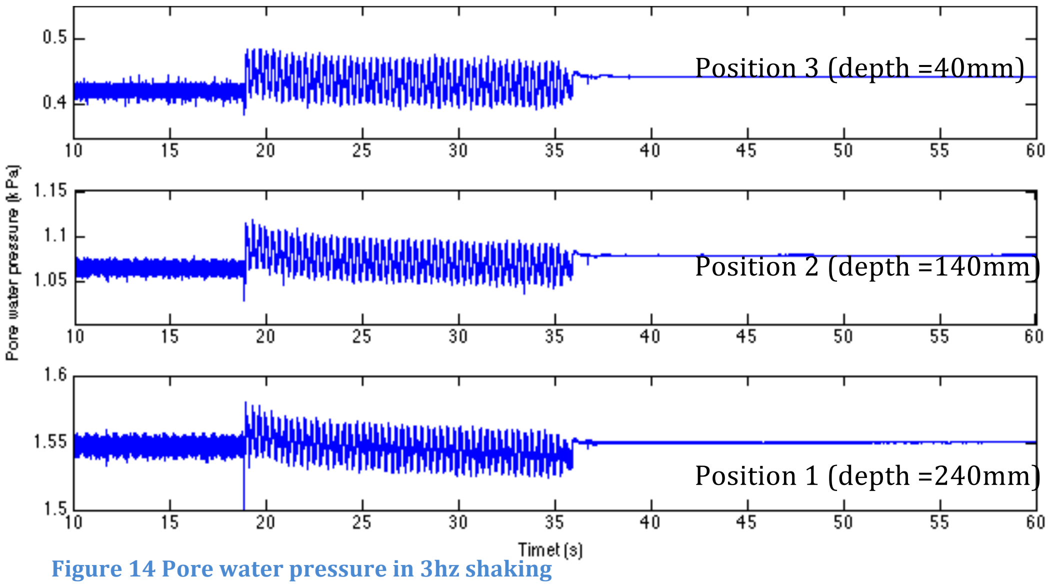

Figure 14 Pore water pressure in 3hz shaking

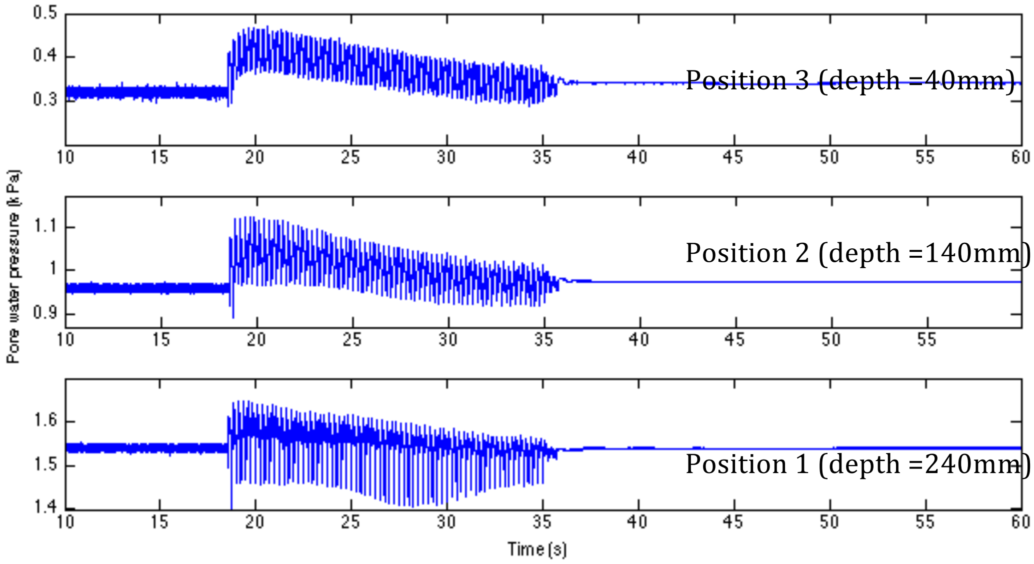

Figure 15 Pore water pressure in 4hz shaking

5.1.2 Effective stress

According to Equation 1 in Section 1, effective stress,σ', in the sample, equals $\sigma - u$. Table 4 shows the minimum effective stress, (i.e. when pore pressure is maximum), at different position in each shaking event.

Location	σ (kPa)	σ'_{2hz}m, (kPa)	σ'_{3hz}m, (kPa)	σ'_{4hz}m, (kPa)
Position 3	0.753	0.383	0.368	0.303
Position 2	2.636	1.511	1.506	1.506
Position 1	4.512	2.952	2.957	2.882

Table 4 Summary of minimum effective stress

Reducing in effective stress and increase in pore water pressure are observed in all the tests, which gives evidences on partial liquefaction. The value of effective stress decreases with the increase in degree of shaking. At position 3, nearest to the top of the soil column, effective stress is minimum with a value close to 0, thus it suffered most severe liquefaction comparing to other locations. According to the visual observation, liquefaction did occur at shallow position. The rough surface of the model is liquefied and leveled, as shown in Figure 16.

Figure 16 Liquefied surface

5.1.3 Settlement

The settlement appears due to dissipation of liquid in sample. It is affected by maximum shear strain, soil density, effective drainage path, etc. By examining the soil profile during the experiments, the total settlement is found to be 2mm, 3mm and 8mm after 2Hz, 3Hz and 4Hz shaking respectively.

The settlement can also be calculated numerically. As a simplified model, the settlement can by estimated by using approximate parabolic isochrones in one-dimensional consolidation. Assume that the drainage path is with the depth of the soil sample in upward direction only. The ultimate settlement, ρ, can be calculated by Equation 12.

$$\rho = \int m_v(\Delta u - \overline{u})dz = \int \frac{(\Delta u - \overline{u})}{E_0}dz \qquad \text{Equation 12}$$

where, E_0 = compression modulus,

and $E_0 = \frac{v\sigma'}{\lambda}$, where v=specific volume, λ=gradient of normal consolidated line.

As there is no experimental data of λ available for Hostun sand, a value for 0.074 (Kuklík (2011)) is selected for estimation purpose. The sample is roughly divided into 3 layers and integrated to give a predicted value of ultimate settlement after 4hz shaking. The value is calculated to be 5.7mm by this method. It roughly agrees with visual observation of 8mm (as shown in Figure 17). A more precise prediction can be achieved by finding actual value of λ for Hostun sand with an tri-axial compression test.

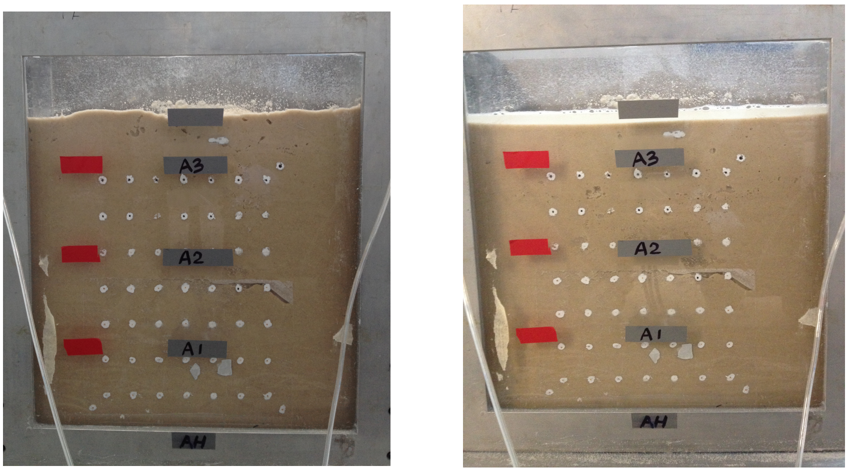

Figure 17 Soil profile (a) before tests (b) after 4Hz shaking

Tokimatsu et al (1987) proposed a chart of simplified relationship between cyclic stress ration,($\frac{\tau_{av}}{\sigma'}$), relative density and volumetric strain for saturated sand. The proposed chart is shown in Figure 6, Section 2.2. By using this chart, with $\tau_{av} = 0.25kPa$, $\sigma' = \gamma' h = 9.3 \times 0.24 = 2.3kPa$, $I_D = 42\%$, the volumetric strain is found to be 3%, giving a settlement of 10.7mm.

5.2 Shear wave velocity

5.2.1 Shear wave velocity prior to shaking

Prior to strong shaking tests, the air hammer was fired to investigate the small strain shear modulus. The air hammer was placed near the bottom of the container and the shear wave generated would propagate upwards. As the shear wave propagates, data recorded by the accelerometers, which are further away from the shear wave generator, will have a reduction in amplitude and a phase shift comparing to adjacent instruments. Shear wave velocity thus can be calculated using the given separation distance between instruments and the phase shift. Both direct arrival method and cross correlation method (using MATLAB code, `xcorr`, is used for finding the lag time. An example is shown below.

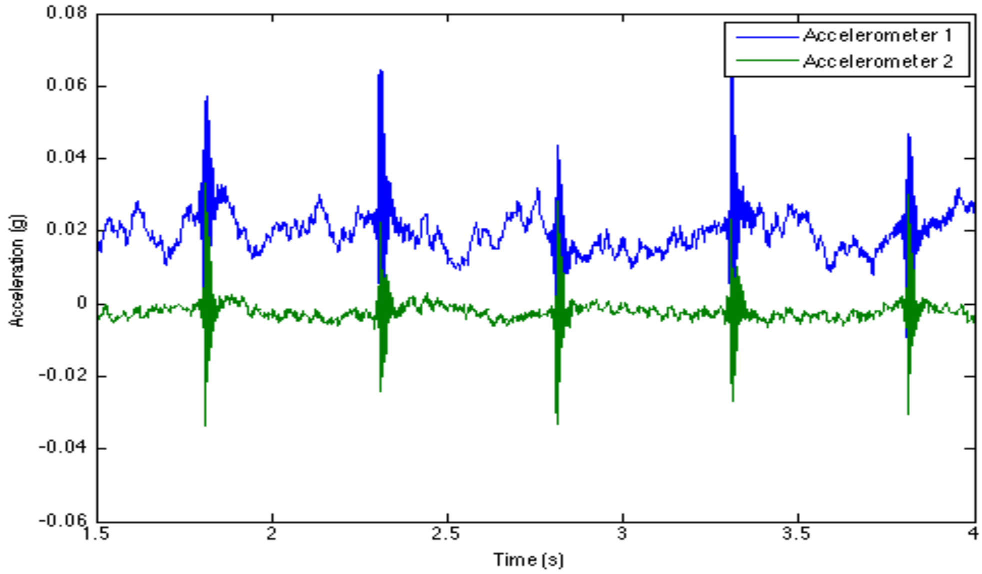

Figure 18 Recorded acceleration when only air hammer is fired

Figure 18 shows presented the result recorded by Accelerometer 1 and 2, the lowest pair of accelerometers with 100mm apart. The distinct pulses shown in the figure corresponds to strokes of the air hammer. Figure 19 presents a close up to one of the pulses. Two similar waveforms with one lagged the other are clearly illustrated. The travel time differences between the arrivals of shear waves at the two accelerometers can be found by examining the difference in x-axis between the peaks of the two signals. Hence,

$$time = 0.0012s$$

The shear wave velocity is estimated by,

$$V_s = \frac{d}{time} = \frac{0.1}{0.0012} = 83.3m/s$$

Initial shear modulus, G_{max}, can therefore be calculated using Equation 6 described in Section 2.3.1.

$$G_{\max} = V_s^2 \rho = 83.3^2 \times 1525 = 10.6MPa$$

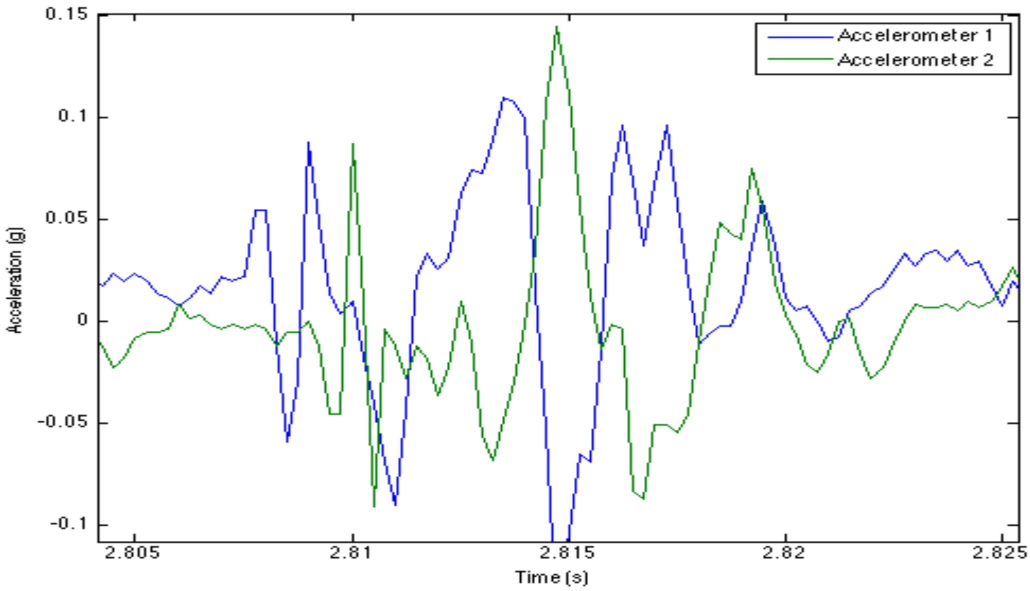

Figure 19 Close-up to one pulse

On the other hand, the shear modulus can be calculated numerically according to Hardin and Drnevich (1972), Equation 5.

$$G_{\max} = 100\frac{(3-e)^2}{1+e}\sqrt{p'} = 100\frac{(3-e)^2}{(1+e)}\sqrt{\frac{1+2K_0}{3}\sigma'_v}$$

where K_0 = coefficient of earth pressure at rest $\approx 1-\sin\phi$

$$\sigma'_v = \gamma' h = \frac{G_s}{1+e}\times\gamma_w h = \frac{2.65}{1+0.74}\times 9.81\times 10^3\times 0.24 = 0.003 MPa$$

$$G_{\max} = 100\frac{(3-0.74)^2}{1+0.74}\sqrt{\frac{1+2\times(1-\sin 35)}{3}\times 0.003} = 13.8 MPa$$

Comparing to experimental result, there is a 23% difference between the results from these two methods. The slight difference may arise from the estimation of shear wave velocity due to the sampling rate. The method is not precise enough for determination of correct shear wave arrival time. Actually, Ghosh (2004) gives figures on % error in the measurement of shear wave velocities in terms of accelerometer distance and sampling rate. In this test, the distance between accelerometers is 100mm and the sampling is 4000hz. Thus, the error will be more than 10%. From Ghosh (2004) it also can be seen that the by increasing the data acquisition rate, the errors associated can be reduced.

5.2.2 Shear wave velocity change due to shaking

During the shaking table tests, the pore pressure accumulated in the voids softens the soil. Thus it becomes more difficult for soil to pick up shear wave. The shear wave velocity will decrease due to this effect. Figure 20, 21 and 22 illustrate typical change in shear wave velocity prior, during and post shaking. The value is calculated by finding the lag time for each loading cycle in a similar manner described in Section 4.2.1. MATLAB (copyright The MathWorks Inc.) code for cross correlation, `xcorr`, is used to give a more precise value in this case.

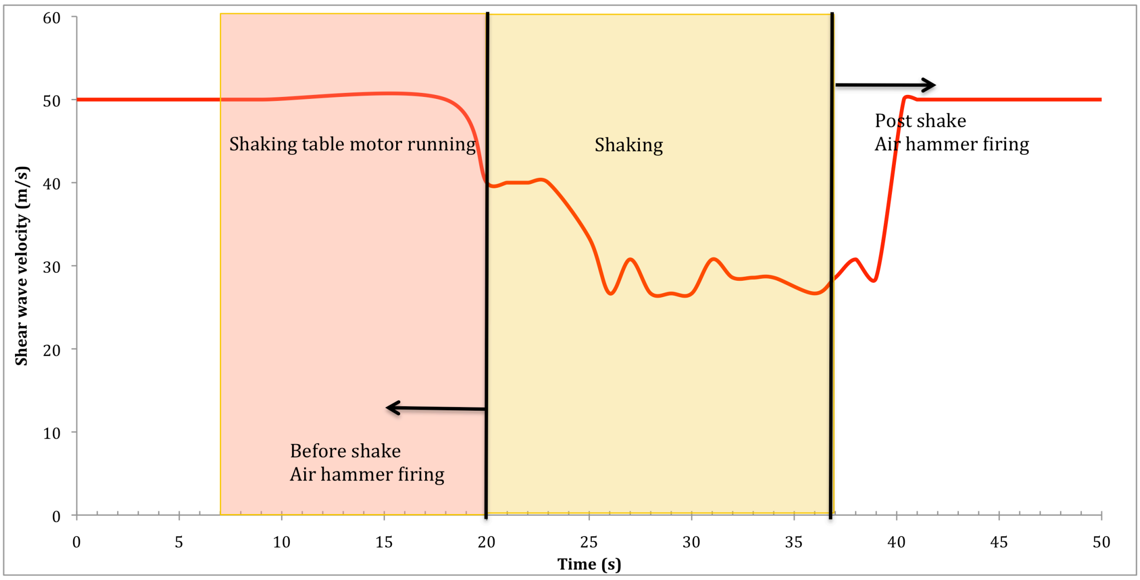

Figure 20 Shear wave velocity change in 2Hz shaking

It can be seen that the shear wave velocity degraded significantly during shaking and appears to increase as the pore pressure is dissipating. From Figure 20 and 21, For relative weak shaking with frequency 2hz and 3hz, as only small excess pore pressure is generated, the soil did not soften too much comparing to 4hz shaking, Figure 22. It should be noted that, before the actual shaking took place, shaking table motor started to running and produced small cyclic vibration in the model. Its effect is not significant in 2hz shaking but noticeable in 3Hz and 4Hz shaking, probably because the vibration is stronger in 3Hz and 4Hz shaking events.

The shear wave velocity is kept above 20m/s during the shaking while the value is close to 10m/s in strong shaking. After shakes, shear velocity in weak shakings managed to recover the shear wave velocity and roughly reached its initial value with a steep gradient. However, in 4Hz shaking with more excess pore pressure, it takes longer for shear wave to recover and the final shear wave velocity only reaches to 60-70% of the value before shaking. The lower post shaking shear wave velocity may be caused due to the change in density of soils under cyclic loading. As shear wave velocity is highly associated with small strain modulus, (i.e. prior or post shaking), it can be predicted that shear modulus will recover to match its initial value after this weak shaking event, but not so much in strong shaking event which will be discussed in Section 5.3.

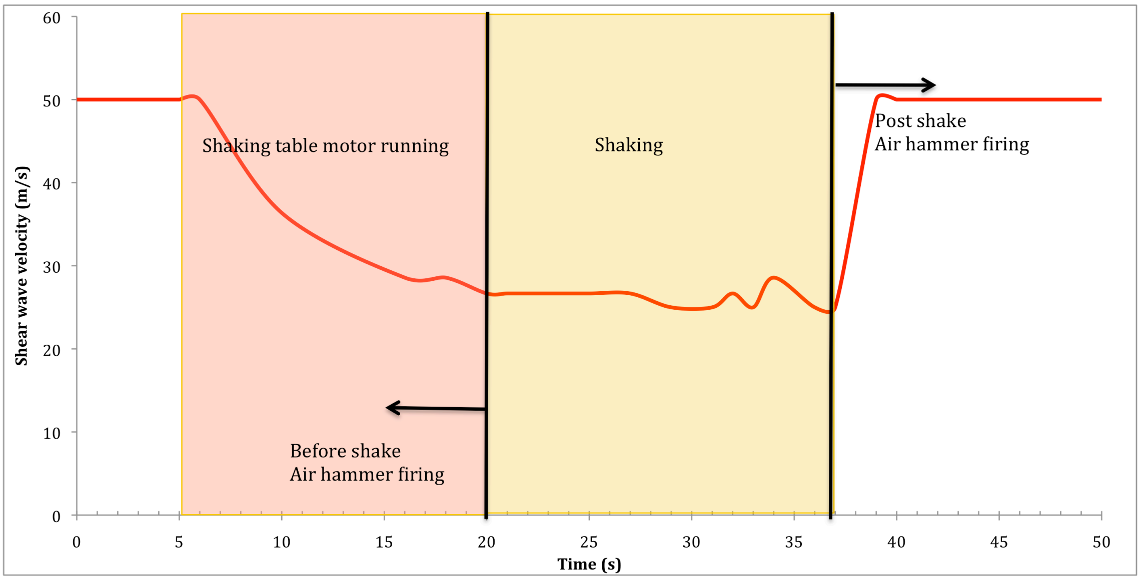

Figure 21 Shear wave velocity change in 3Hz shaking

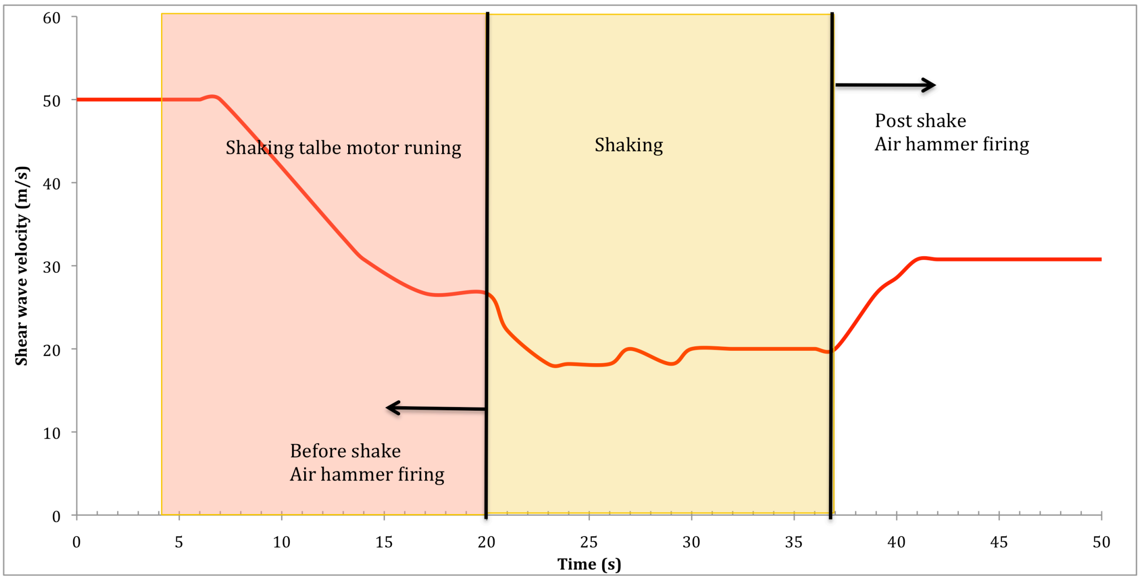

Figure 22 Shear wave velocity change in 4Hz shaking

5.3 Soil stiffness degradation

5.3.1 Stress-strain loop

During dynamic events, continuous monitoring stiffness of soil is necessary and important to predict the soil behaviour. A MATLAB (copyright The Mathworks Inc.) code is used to draw stress-strain loop during the shaking. The code is written based on the theory described in Section 2.3.2. Figure 23, 24 and 25 below show the stress-strain loops at 2s, 5s, and 10s for 2Hz, 3Hz, and 4Hz shaking respectively. The dash lines indicate the representative shear stiffness in the loops.

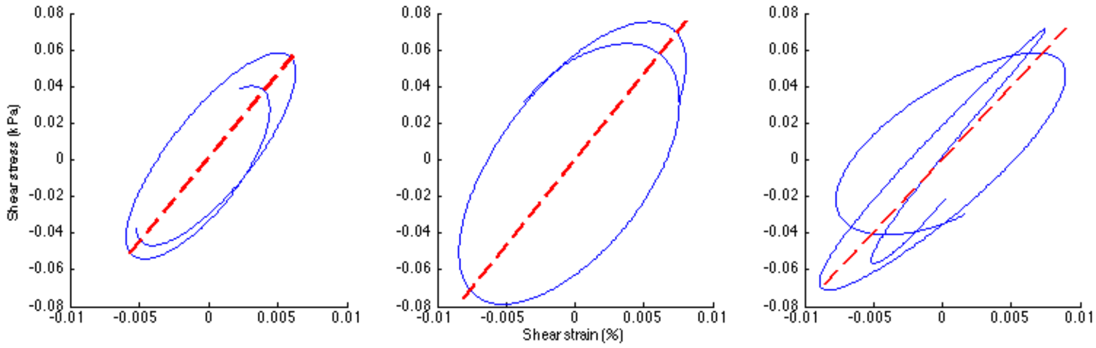

Figure 23 Stress-stress strain loop at 2s, 5s, and 10s for 2Hz shaking

For 2Hz shaking experiment, the gradient on stress-strain loop does not flattened significantly at 10s loop, indicating that there is no significant degradation in soil modulus. The shear strain induced in 2Hz shaking event is roughly in the range of 0.01%, which is very small. Hence, the small strain shear modulus calculation may still applicable. The result is reasonable given that 2Hz shaking is the weakest shaking event. The pore pressure generated due to this event is insignificant. Hence, there is little change in shear modulus and the effect of liquefaction with the relative small shear strain induced by the shaking is not obvious, which agrees with the observation during the experiments. Due to the small strain, the soil should still behave linearly and elastically, although the stress strain loops shows hysteretic behaviour. This could be a result of sliding effects mentioned in Section 4.

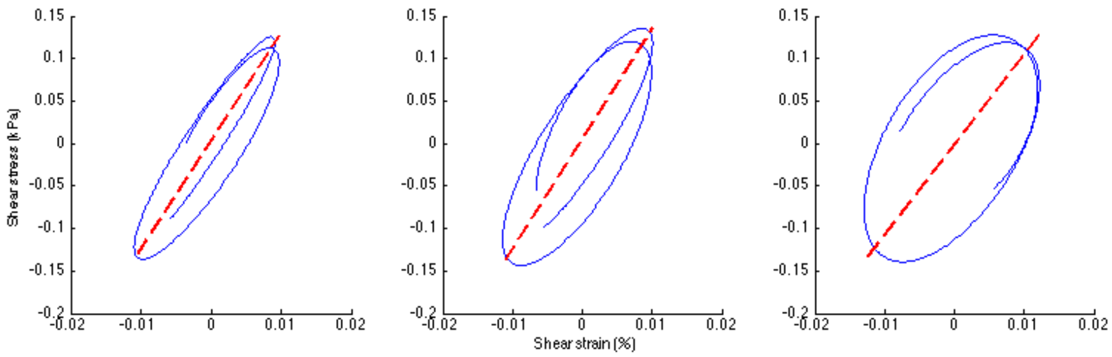

Figure 24 Shear strain loops at 2s , 5s and 10s in 3Hz shaking

In 3Hz and 4Hz shaking evens, the shear strain range is increased to 0.02% about twice comparing to 2Hz event. The graphs in Figure 24 and 25 demonstrates a more obvious closed stress-strain loop. Also, the reduction in gradient is more noticeable in Figure 24. Sand is noticed to be softened and liquid dissipated from the voids started to come out from the top of the container through visual observations.

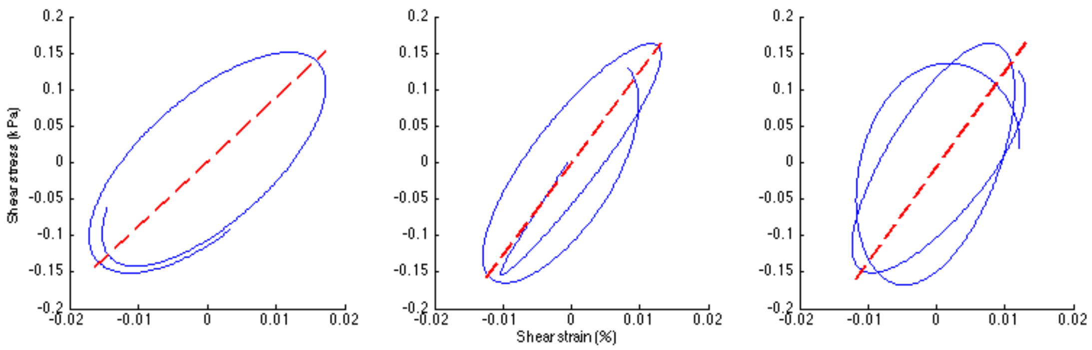

Figure 25 Stress strain loop at 2s, 5s and 10s in 4Hz shaking

In 4Hz shaking event, from 2s to 5s, the gradient on stress-strain loop even increases. This can be explained by the increase in density. The relative density increases after previous shaking events. The denser sands tends to dilate when the shaking continues. The regain in stiffness is due to associated dilative tendency (Elgamal et at. (2005)).

Under cyclic loading, the shear stress and strain calculation and thus the shear modulus are heavily dependent on the acceleration data recorded, as discussed in Section 2.3.2. Especially for shear strain, as it is found by integration of accelerations. The sliding effect mentioned in Section 4, which is not completely removed by filtering, has some effects to the accuracy, and may lead to a result that is difficult to interpret the meaning.

After the experiments, soil models were excavated. Evidence has been found on sliding with some of the instruments being shifted by around 10mm.

5.3.2 Shear modulus recovery

Figure 26, 27 and 28 show the recovery of shear modulus over time in 2hz, 3hz, 4hz shaking respectively. For period before or after shaking, the shear modulus is calculated by Equation 6. As for the shaded shaking area, shear modulus is calculated by working out the gradient of stress-strain loop. The y-axis indicates the shear modulus normalized with its initial value.

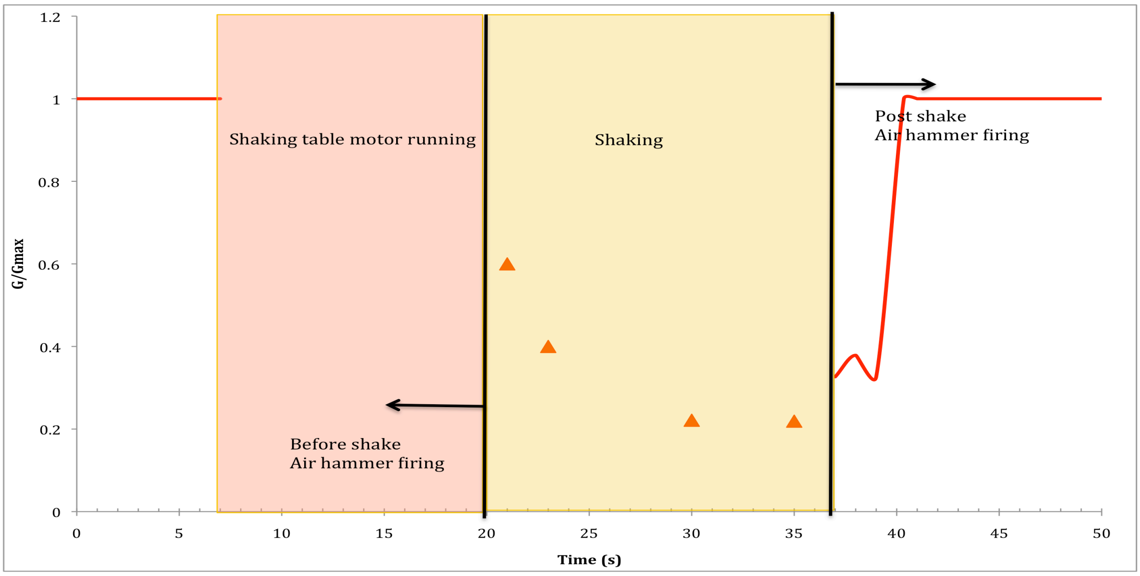

Figure 26 Shear modulus change in 2Hz shaking

Comparing with the shear velocity diagram in Section 4.2.2, shear modulus curve shows similar trend lines. Soil is softened during the shaking, as it is partial liquefied. As can be seen in Figure 26, the soil is stiffer initially. When shaking started, the shear modulus degraded gradually with time, which means that the soil experienced more liquefaction with increasing number of loading cycles. In Figure 27 and 28 the soil experience a sudden drops in shear modulus right after the shaking started, which will cause severe damages if structure were loaded on the soil. Moreover, the shear modulus degraded more significant than in 2hz shaking due to stronger shaking thus more liquefaction. For 4Hz shaking event, the shear modulus regained, during the shaking stage, this can be caused by the dilative effect or sliding of instruments.

After 2Hz and 3Hz shaking event, the modulus recovered to original state while the residual shear modulus for 4Hz shaking remained at around 60% of its original value. The reduction in shear modulus is partially because that the permanent change in density is not taken into account.

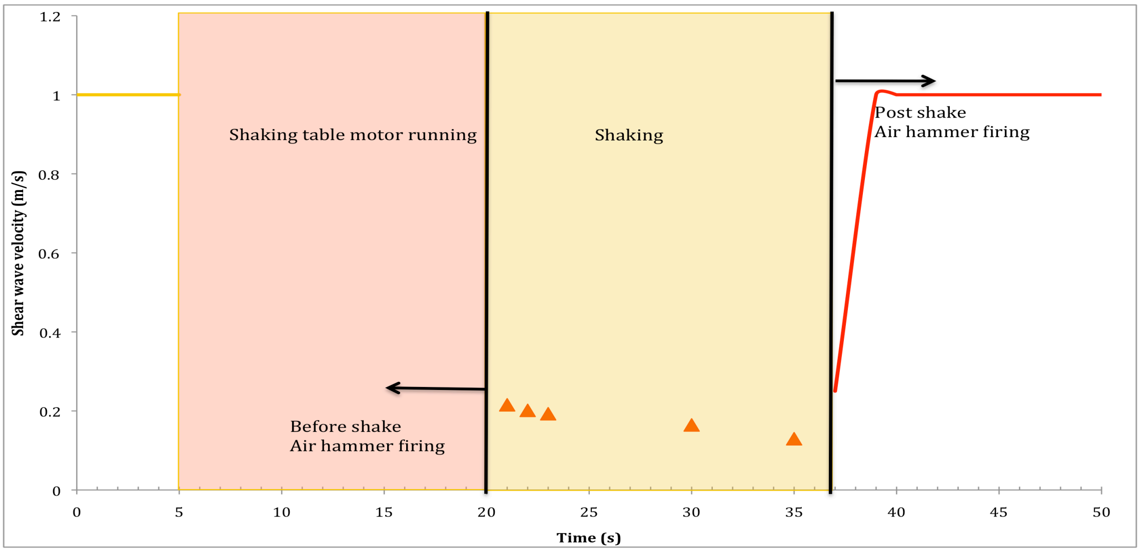

Figure 27 Shear modulus change in 3Hz shaking

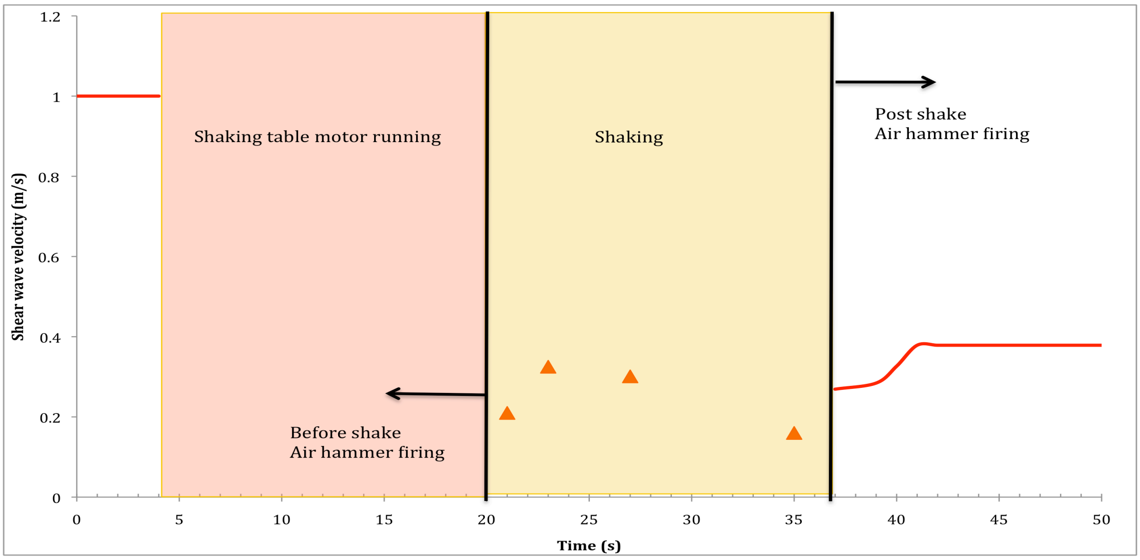

Figure 28 Shear modulus change in 4Hz shaking

Figure 29 on next page shows the change of shear modulus according to the shear strain together with predicted value by Hardin and Drevich (1972). Although it is only plotted over a small range of strain, it shows that value predicted by Hardin and Drevich is stiffer.

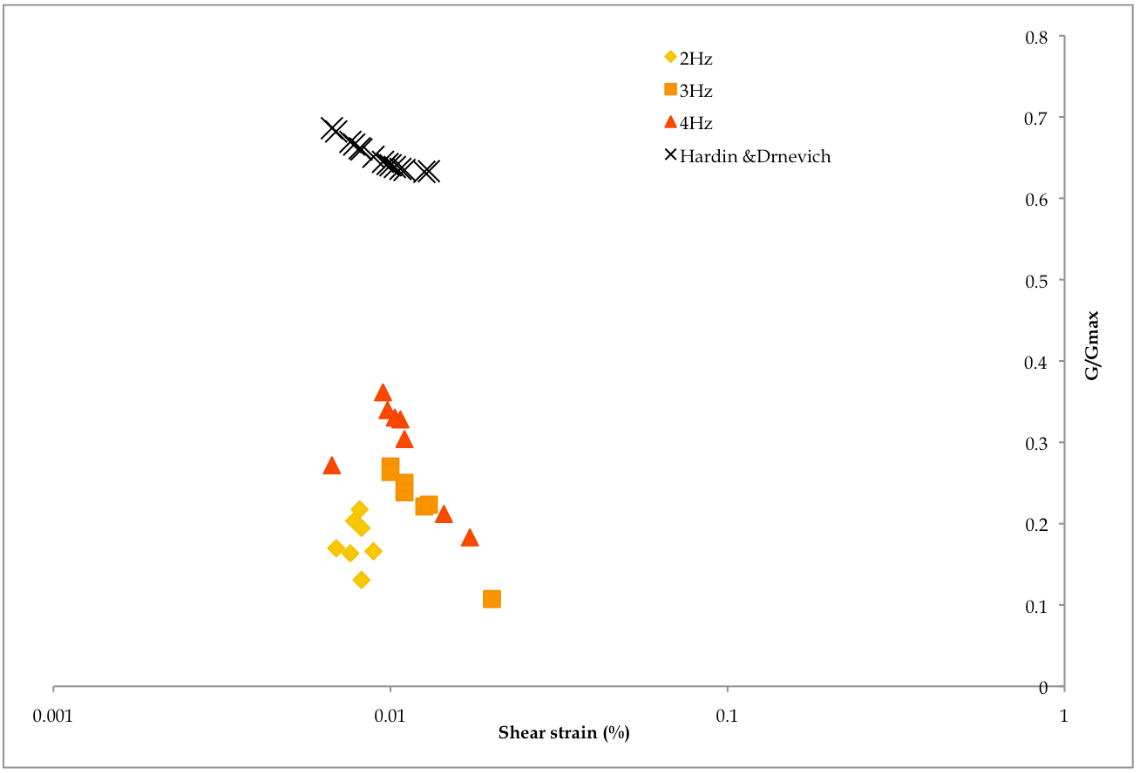

Figure 29 Shear modulus vs. shear strain

6 RESULTS OF LAYERED SAND MODEL

In the layered sand, two different soil behaviours was observed in sand and clay layer. There almost was no increase in pore water pressure recorded but the shear modulus did degrade during shaking. This may be because the insensitivity of PPTs used. Due to the weight of clay, sand has settled a little prior to the tests and the total settlement due to shaking is 2mm, comparing to 8mm in homogeneous model. Sand layer is considered to contribute most to this settlement as clay has very low permeability and the water will take much longer time to dissipate.

6.1 Shear wave velocity

6.1.1 Shear wave transmission in different soils

The clay used in this experiment is very soft with a lot of water content. It has very little strength and are difficult to transfer shear wave. Figure 30 shows how signal propagates through different soils. Figure 30(a) illustrates two signals in Hostun sand. The signal arriving at accelerometer 2 keeps the form shape with little time delay. Figure 30(b) shows the signal at accelerometer 2 and 3. The signal delay is found out to be 0.01s, comparing to less than 0.002s in (a). Meanwhile, the amplitude of the signal is dramatically reduced by about three quarters. This example shows that shear wave transition is heavily dependent on water content in the soil. Hence, when the soil liquefied during shaking, the shear wave velocity decreases.

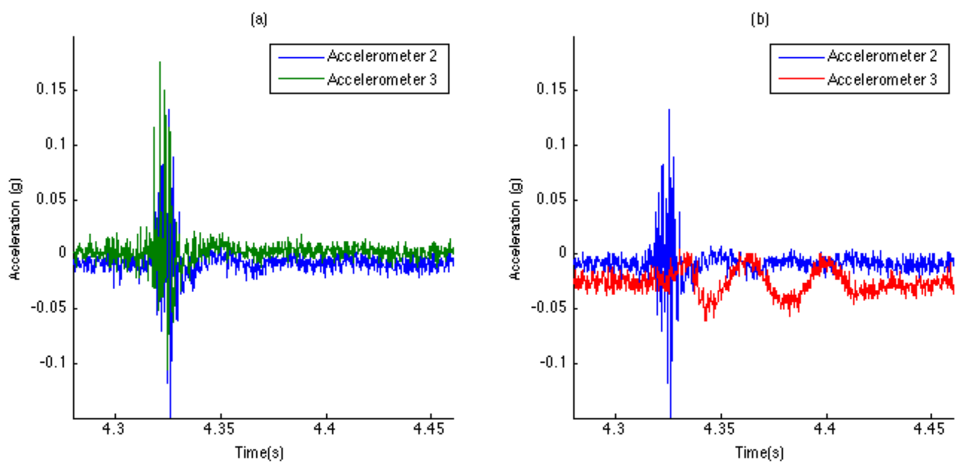

Figure 30 Shear wave velocity transmitted in (a) sand (b) clay

6.1.2 Shear wave velocity change due to shaking

Figure 31 shows how the shear wave velocities change due to 4Hz shaking in two soil layers. In sand layer, a similar result is got as Figure 22 in Section 5.2.2. As the sand is denser in this case, the initial shear wave velocity is greater than that in loose sand, which shows that the shear wave propagates faster in dense sand as the soil is more compacted with less water content in voids and there are more solid soil particles to pick up the shear wave.

As for the clay, the shear wave velocity keeps at an almost constant value, which is much smaller than that in dense sand. According to pore pressure data, there is no significant excess pore pressure generated, hence the soil stiffness is not largely degraded, giving a similar value of shear wave velocity before and after the shakes.

Roughly combine the two soil effects by consider it as one uniform soil. The shear wave velocity is estimated by the separation distance and travelling time between Position 1 and 3. The value for the 'combined' effect is represented by green line in Figure 31. According to the graph, the line is more similar to the one for clay layer. In the 'combined' model, sand layer only contributes little as it travels very fast, which means the shear wave is transmitted at an almost doubled speed. It seems that clay dominates the layered soil behaviour although it only accounts for one third of the volume. Although there is almost no decrease in shear wave velocity, the value is even lower than the degraded value in sand for the whole experiments, which is not useful for supporting structures.

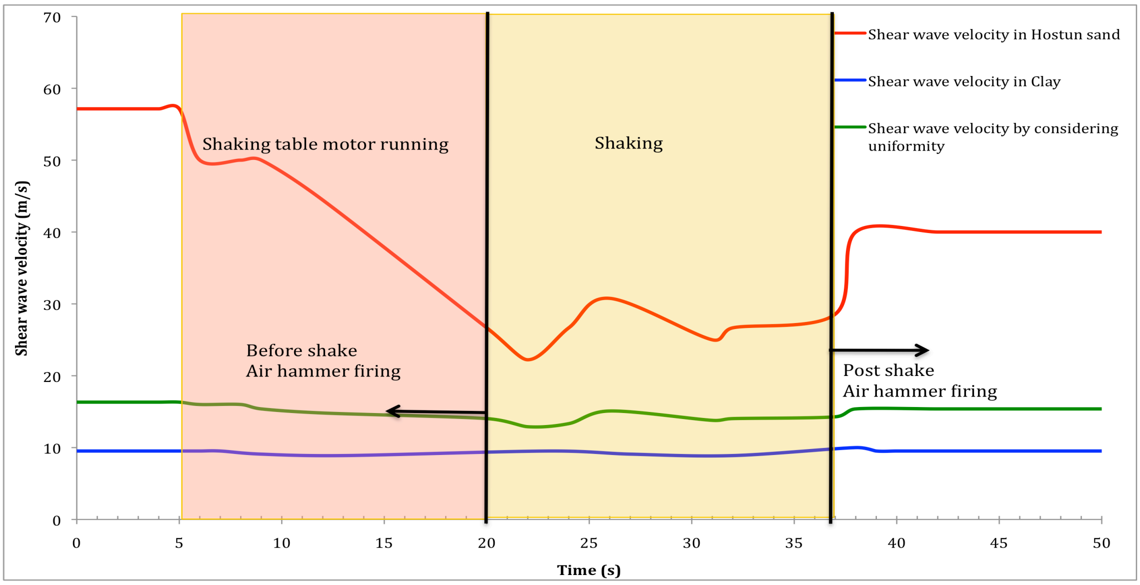

Figure 31 Shear wave velocity change in 4Hz shaking

6.2 Shear modulus degradation

6.2.1 stress strain loop

Figure 32 and 33 show the stress strain loops at 4Hz shaking in modulus degradation of the sand and clay at 2s, 5s and 10s in 4hz shaking respectively. During the analysis, only a first order approximation of strain (Equation 10) is applied in both layers due to the limitation on number of instruments. In sand layer, the shear modulus degraded as the shakes continuous. In first a few seconds, the sand is strongly sheared, resulting in a reduction in shear modulus. As the shake continues, the soil densified and the rate of change in shear modulus is decreased. As the send is denser, the shear strain induced is very small, only in the range of 0.005%.

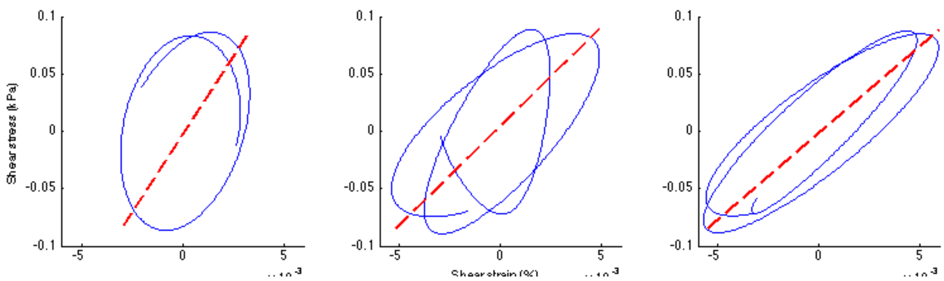

Figure 32 Stress strain loops at 2s, 5s and 10s in sand layer at 4Hz shaking

On the other hand, the stress-strain loop for clay is much more narrow than sand. This can indicate that clay has a smaller damping ratio than sand. The assumption is reasonable as clay is more continuous than sand and the loading cannot be quickly dissipated into the surroundings. (Tohwata, (2008)). As the clay is softer, it is free to move around. The shear strain induced is almost 10 times larger than that in sand.

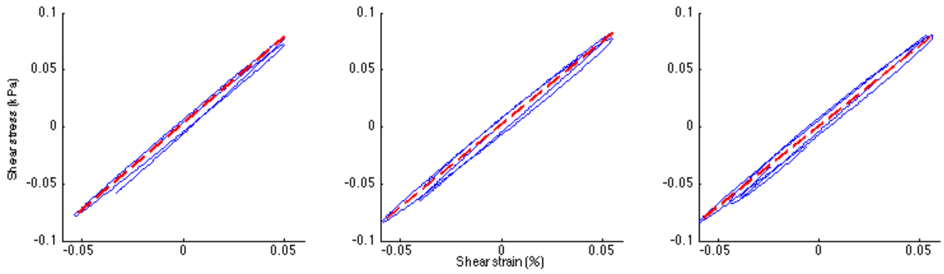

Figure 33 Stress strain loops at 2s, 5s and 10s in clay layer at 4Hz shaking

6.2.2 Shear modulus recovery

Figure 34 shows the degradation and recovery of shear modulus is sand and clay. The shear modulus is normalized with it is initial value. Similar to homogenous sand, both in sand and clay layer, the shear modulus decreases during the shake and recovers afterwards. In clay layer, the shear modulus only degrades to 80% of its original value and managed to get a full recovery at the end. However, in sand layer, the shear modulus drops to 20%. During the shaking process, the clay sometimes regains a small amount of stiffness. This is may be caused by the sliding effects mentioned in Section4. As the clay is soft and the effective vertical stress is small comparing to sand, the sliding effect at shallow level is more likely to happen than at deep levels.

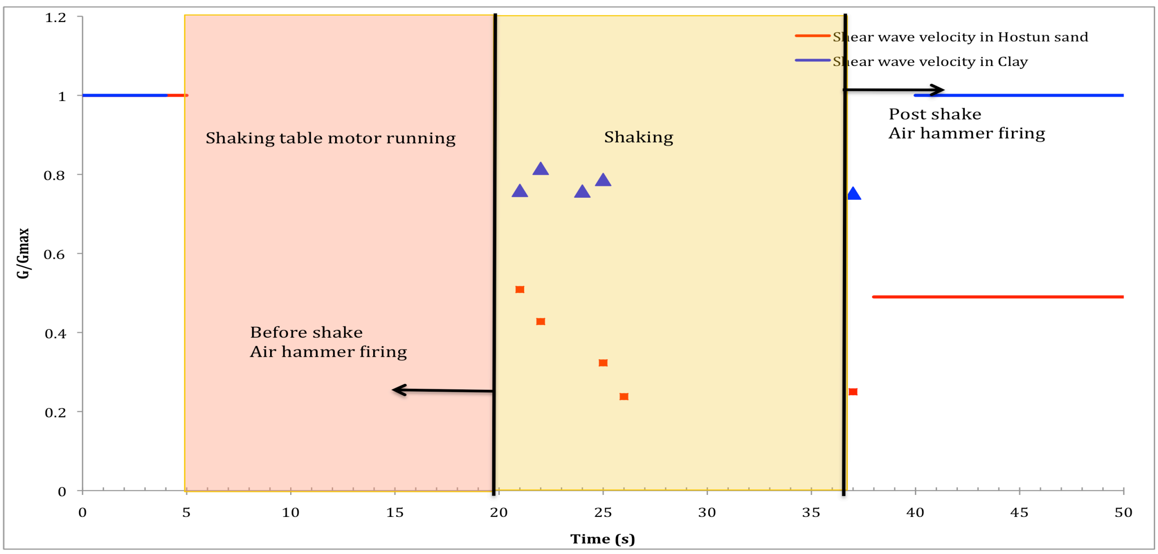

Figure 34 Shear modulus change in 4Hz shaking

Figure 35 plots the normalized shear modulus with the strain. As the experiments only operated in small scale, the variety of shear strain is limited. Hence, the data from the experiments only lie within a narrow band. The experimental data is compared with Hardin and Drvenich(1972)'s expression. It is found out that their expression tends to have a larger overestimate if the shear strain is small. Brennan et al. (2005) found the same results by centrifuge tests.

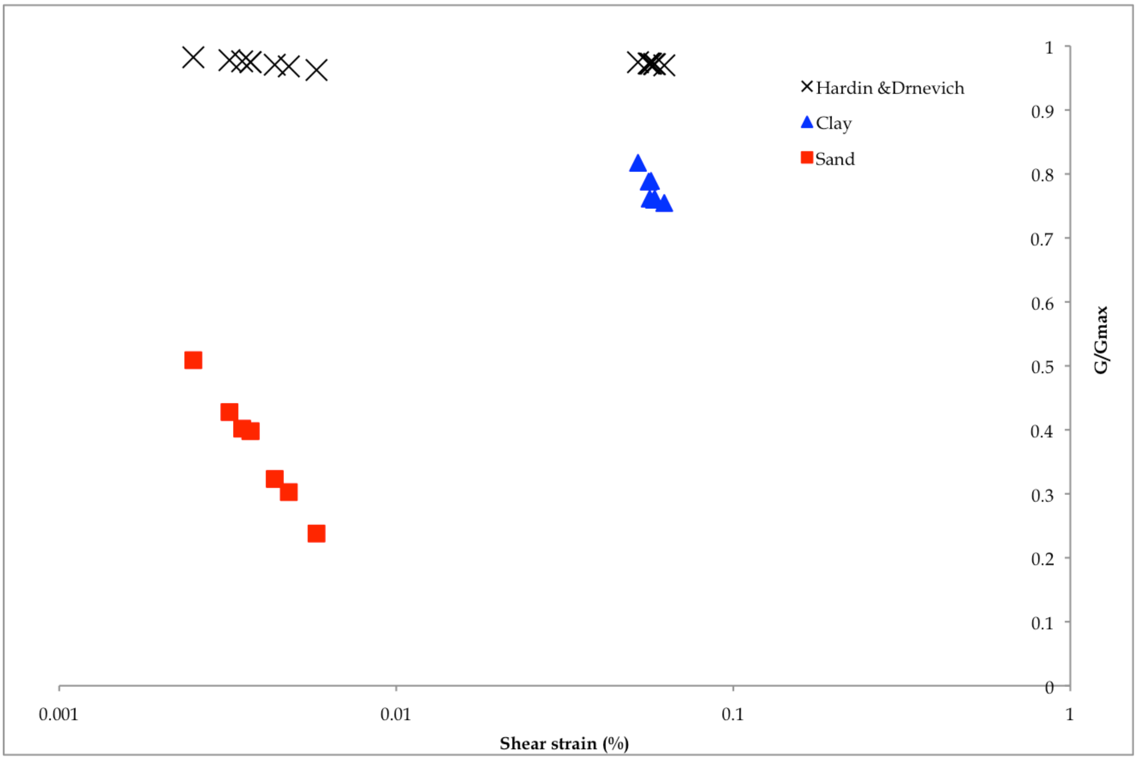

Figure 35 Shear modulus vs. shear strain

7 CONCLUSION

Air hammer and 1-g shaking table were used during the experiment to find shear modulus. For small strain modulus, before and after the shaking, air hammer was fired alone and the shear modulus can be found by measuring the shear wave velocity. Similar works have been done by Ghosh and Madabhushi (2002). For large strain modulus, 1D shear beam equation is modified to find stress and strain. Shear modulus can be found by working out the slope of shear strain loop. It is proved that this method is efficient and gives appropriate value on shear modulus.

However, there are several aspects that need to pay particular attention of. During the data logging process, the sliding of accelerometers can significantly affect the results. Instead of recording a sinusoidal signal, the instruments tend to record a distorted square wave. As the stress and strain is calculated based on accelerations, the resulting stress-strain loop will be meaningless. The sliding effect is more significant in liquefied area. Thus, the data needs to be handled properly, especially for the filtering of the data. Specific band filter is designed using MATLAB, which gives a neater signal with useful information still preserved.

Pore water pressure accumulated in loose sand is clearly recorded and observed. On the other hand, in layered model, there is no obvious excess water pressure during both clay and sand models. This can be a result of insensitive instruments or not strong enough shaking is applied to the model. The settlement of the final soil profile is caused due to the dissipation of excess pore pressure. The visual observation is compared with parabolic isochrones approximation and Tokimatsu et al.(1987). The visual results show a reasonable agreement with both of them. As water is used as pore liquid, the settlement occurred almost immediately after the shaking. A more viscous fluid can be used if more detailed investigations need be done on pore pressure.

Shear wave velocity is calculated using simple equation of distance of shear wave over travelling time. However, it is not easy to find accurate values on travelling time. Both cross-correlation and direct arrival method were used. In layered models, it if found out that the clay will reduce the amplitude shear wave transmitted and has a significant delay in the shear wave arriving time. This may be due to the large water content in clay, which cannot carry significant amount of shear. The experimental data shows in sand, the shear wave velocity drops significantly in shaking but recovered afterwards and so does the shear modulus. While in clay, the shear wave velocity almost does not change but the shear modulus does degrade. The resulting permanent lose of shear modulus is caused by not taking into account the compaction of sands after shakings. The shear modulus degraded is compared with Hardin and Drevench(1972). Although the variation in shear strain is not large enough due to the limitation of experiments, it indicates that Hardin and Drevench (1972)'s equation tends to overestimate the shear modulus over small shear strain.

By considering the layered sand as one uniform sample, it is found out that the shear wave velocities hence shear modulus before and after shaking behaves more like clay and there is great decrease stiffness. The clay seems to change to soil behaviour although in only takes up one third of the volume. This may be caused as the clay used is far too soft than sand. Stiffer clay may be used to investigate the degree of influence caused by soft soil.

8 REFERENCES

1 A.J. Brennan, N.I. Thusyanthan and S.P.G. Madabhushi. "Evaluation of shear modulus and amping in dynamic centrifuge tests." *Journal of geotechnical and geoenvironmental engineering* 131 (2005): 1488-1497.

2 Ahmed Elgamal, Zhaohui Yang, Tao Lai, Bruce L. Kutter and Daniel W. Wilson. "Dynamic response of saturated dense sand in laminated centrifuge container." *Journal of geotechnical and geoenvironmental engineering* 131 (2005): 598-609.

3 B. Ghosh, S.P.G. Madabhushi. "An efficient tool for measuring shear wave velocity in the cetnrifuge." *International conference of physical modelling in geotechnics.* 2002. 119-124.

4 B. O. Hardin, V.P.Drnevich. "Shear modulus and damping in soils: measurements and parameter effects (Terzaghi Lecture)." *Journal of soil mechanics foundation division* 98 (1972): 603-624.

5 G. Viggiani, J. H. Atkinson. "Interpretaion of bender element tests." *Geotechnique*, 1995: 149-154.

6 Ghosh, Barnali. "Behaviour of rigid foundation in layered soils during seismic liquefaction." PhD thesis, Engineering Department, Cambridge Unversity, 2004.

7 H.B. Seed, K. TOKIMATSU, L. Harder. "The influence of SPT procedures in evaluating soil liquefaction resistance." University of California.

8 Ishihara, K. "Stability of natural deposits during earthquake." *Proceedings XI international conference on soil mechanics and geotechnicall engineering.* 1985.

9 K. Tokimatsu, Y. Yoshimi. "Criteria of soil liqeufaction with SPT and fines content." *Proceedings of world conference on earthquake engineering.* 1984.

10 K.L. Lee, A. Albaisa. "Earthquake-induced settlements in saturated sands." *Journal of soil mechanics foundation division* 100 (1974): 387-400.

11 Kohji Tokimatsu, Bolton Seed. "Evaluation of settlements in sands due to earthquake shaking." *Journal of geotechnical engineering* 113 (1987): 861-878.

12 Kuklík, Pavel. "Preconsolidation, structural strength of soil, and its effect on subsoil upper structure interaction." *Engineering Structures* 33 (2011): 1195-1204.

15 M. Zeghal, A.W. Elgamal. "Analysis of site liquefaction using earthquake records." *Journal of geotechnical engineering* 120 (1994): 996-1017.

16 Meyerhof, G.G. "Discussion." *Proceedings of 4th international conference of soil mechanics foundation engineering.* 110.

17 Newland, D. E. *Newland D.E (2005) An introduction to random vibration, spectural and wavelet analysis.* 2005.

18 Randell, Helen. "Soils stiffness before and after liquefaction." Fourth-year under graduate project, Engineering Department, Cambridge University, 2010.

19 Towhata, Ikuo. *Geotechnical earthquake engineering.* 2008.

20 Yasuyuki Koga, Osamu Matsuo. "Shaking talbe tests of embankment resting on liquefiable sandy ground." *Soils and foundations* 30 (1990).